JOURNAL OF SPACECRAFT AND ROCKETS
Vol. 42, No. 1, January–February 2005

Robust Control for Microgravity Vibration Isolation

Mark Whorton*
NASA Marshall Space Flight Center, Huntsville, Alabama 35812

Many microgravity science experiments need an active isolation system to provide a sufficiently quiescent acceleration environment. The glovebox integrated microgravity isolation technology (g-LIMIT) vibration isolation system will provide isolation for microgravity science glovebox experiments in the International Space Station. Although standard control system technologies have been demonstrated for these applications, modern control methods have the potential for meeting performance requirements while providing robust stability in the presence of parametric uncertainties that are characteristic of microgravity vibration isolation systems such as g-LIMIT. Whereas H_2 and H_∞ methods are well established, neither provides the levels of attenuation performance and robust stability in a compensator with low order. Mixed H_2/μ controllers provide a means for maximizing robust stability for a given level of mean-square nominal performance while directly optimizing for controller order constraints. The benefit of mixed norm design is demonstrated from the perspective of robustness to parametric uncertainties and controller order for microgravity vibration isolation. A nominal performance metric analogous to the μ measure for robust stability assessment is also introduced to define an acceptable trade space from which different control methodologies can be compared.

Nomenclature

$A, B_p, B_1, B_2, C_p, C_1, C_2, D_{1p}, D_{12}, D_{2p}, D_{21}, D_{22}$	=	generalized plant coefficient matrices
$\bar{A}, \bar{B}_p, \bar{B}_1, \bar{B}_2, \bar{C}_p, \bar{C}_1, \bar{C}_2, \bar{D}_{1p}, \bar{D}_{12}$	=	augmented system coefficient matrices
G	=	optimal control gain matrix
H_∞, H_2	=	Hardy spaces
$\mathcal{L}$	=	mixed-norm Lagrangian
$\boldsymbol{T}_{zw}$	=	closed-loop transfer function from z to w
μ	=	structured singular value

I. Introduction

CONDUCTING research in a low-acceleration environment enables scientific investigations that are not possible on the surface of the Earth. Entirely new research directions are being developed for pursuit in low Earth orbit in disciplines such as life sciences, materials science, combustion, fundamental physics, and fluid mechanics. When completed, the International Space Station (ISS) will be a unique research laboratory for state-of-the-art microgravity science investigations.

Yet due to a variety of vibroacoustic disturbances on ISS, the acceleration environment is expected to exceed significantly the requirements of many acceleration-sensitive experiments. Figure 1 presents an estimate of the acceleration environment on the ISS at assembly complete, which exceeds the required acceleration levels for microgravity science at virtually all frequencies. Mitigation of the excessive acceleration environment requires the implementation of vibration isolation systems at either the disturbance source location or the payload location. Whereas an effort is being made to limit the induced disturbances, the ubiquitous nature of disturbance sources necessitates the use of vibration isolation at the payload/rack locations.

A. Isolation Performance Requirement

Much like traditional flexible space structures, microgravity vibration isolation is a challenging structural control problem due to the stringent performance requirements. The isolation system must sense and cancel accelerations with a magnitude of 1,000,000th the acceleration of gravity at the surface of the Earth ($1\ \mu g$) occurring over tens of seconds. This low-frequency attenuation is typically accomplished with high-gain acceleration feedback. Some payloads also require command tracking or cancellation of direct disturbance forces at frequencies of tens of hertz, thus necessitating high bandwidth control.

By the comparison of the ISS acceleration requirement with the expected ISS acceleration environment, an isolation performance specification can be derived. True inertial isolation is neither desirable nor possible due to the large-amplitude motion of the ISS from low-frequency gravity gradient and aerodynamic torques. At these low frequencies, the isolated experiment must move with the ISS and the isolation system must directly transmit the very low-frequency quasi-steady accelerations of the vehicle to the isolated assembly. Figure 1 implies that the isolation system must attenuate the ambient ISS accelerations by one order of magnitude at 0.1 Hz, which for a second-order system implies a maximum break frequency of 0.01 Hz. This break frequency is constrained from below as well by the "rattle space," an envelope of relative motion between the isolated experiment and the moving ISS support structure. Hence, the isolation system must pass through accelerations below 0.01 Hz and attenuate disturbances above 0.01 Hz. An isolation system that satisfies this attenuation function would reduce the anticipated ambient environment sufficiently to provide the required environment at the payload location.

B. Modeling and Robustness Issues

Model uncertainties are a significant aspect of the control system design for microgravity vibration isolation systems. Utility umbilicals are typically the only physical connection between the isolated subsystem and the fixed subsystem of a vibration isolation system. Because it is the primary load path for disturbances to the platform, these umbilicals are designed to have low stiffness and damping properties.[1] (High passive damping adversely affects attenuation above the system natural frequency.) Stiffness and damping estimates can be measured in constrained three-degree-of-freedom

Received 23 July 2003; presented as Paper 2003-5422 at the AIAA Guidance, Navigation, and Control Conference, Austin, TX, 11–14 August 2003; revision received 11 December 2003; accepted for publication 5 January 2004.

*g-LIMIT Principal Investigator, Space Transportation Directorate, Guidance, Navigation, and Control Systems Group; mark.whorton@nasa.gov. Associate Fellow AIAA.

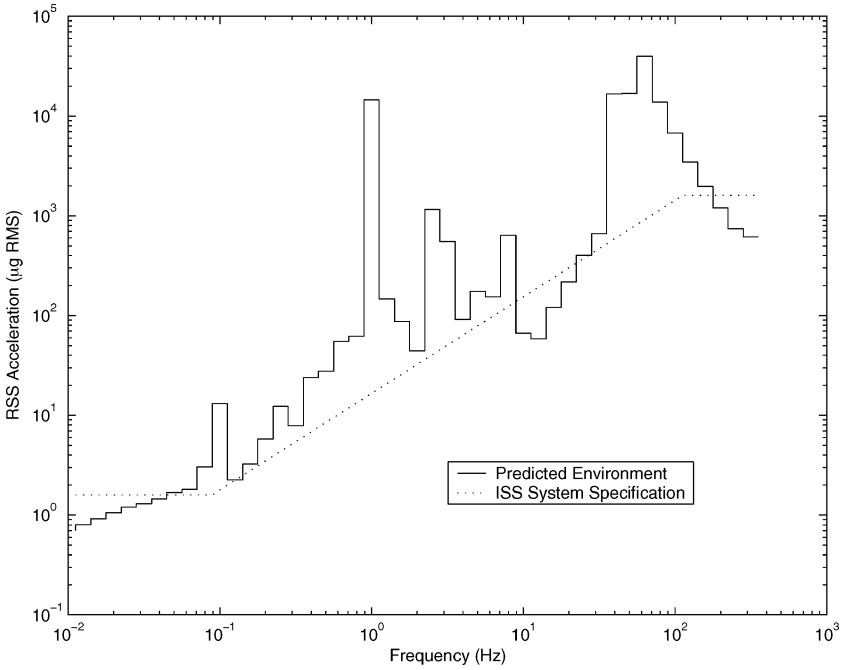

Fig. 1 Predicted rms acceleration environment of ISS in microgravity.

testing, but the full stiffness and damping matrices of the system cannot be accurately measured on the ground due to gravitational deflections and coupling. Hence, not only are umbilicals the primary load path, they are also the primary uncertainties for control system design.

Microgravity vibration isolation systems are typically modeled as a six-degree-of-freedom spring–mass–damper system with either rigid or flexible structural dynamics. Whereas control system design for rack-level isolation systems is a challenge due to the flexibility of the isolated rack structure, the large mass of the rack typically permits passive isolation in the frequency range of the rack structural dynamics. A different challenge is posed by payload-level isolation systems. Whereas the structure is essentially a rigid mass on a flexible spring, the payload mass is on the same order of magnitude as the isolation system. The isolation system must accommodate the significant mass and inertia variations as various experiments utilize the isolation system during its operational lifetime. Because the ratio of payload mass to the payload isolation system mass is nearly one, mass and inertia variations are a much more significant issue for payload isolation systems than for rack-level isolation systems. In both cases, uncertainty due to unknown payload structural dynamics must also be considered.

C. State of Applied Control Systems Technology

Most flight systems to date have used classical control methods.[2,3] These applications neglect the multivariable nature of the problem that arises through the distributed sensing, actuation, and dynamic coupling. Modern control methods are well suited for these multivariable systems and limited applications of H_2 and H_∞ control methods to microgravity vibration isolation have been addressed in design studies. H_2 methods have been fruitfully applied for nominal performance,[4–6] whereas H_∞ methods have been used for robust stability to parametric uncertainties[6] and high-frequency unmodeled modes.[7] However, H_2 methods do not meet performance requirements with acceptable stability properties, nor did they address implementation issues such as compensator dimension. H_∞ methods are promising for stability robustness, but the controller dimension in previous studies is too large to implement in actual flight systems.

The need to satisfy an H_2 performance metric while maximizing stability robustness is addressed by recent developments in the mixed H_2/H_∞ control methodology. This methodology is especially well suited for microgravity vibration isolation by designing high-performance controllers of fixed dimension with guaranteed robust stability constraints. This approach is also significant from an implementation aspect because the controllers are optimized subject to a fixed controller state dimension. In this paper, fixed-order mixed norm controllers are designed for glovebox integrated microgravity isolation technology (g-LIMIT), a payload-level isolation system. These mixed norm control designs are contrasted with standard H_2 and μ controllers from the perspectives of nominal performance and robust stability to parametric structured uncertainties.

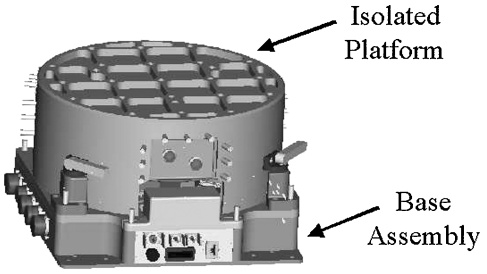

Fig. 2 System assembly of g-LIMIT.

II. g-LIMIT System Description

The g-LIMIT system is a microgravity vibration isolation system designed and built by NASA Marshall Space Flight Center to provide active vibration isolation for microgravity science payloads on ISS.[8] Shown in Fig. 2, g-LIMIT is scheduled for launch on the Utilization and Logistics Flight-1 (ULF-1) mission to the ISS and will commence characterization testing in the microgravity science glovebox (MSG) shortly thereafter.

A. Hardware Description

To provide a quiescent acceleration environment to an experiment, an isolation system must sense and cancel the inertial accelerations applied to the experiment. The g-LIMIT system accomplishes this inertial isolation with six independent control actuation channels that provide six independent forces to the platform on which the experiment is attached. Figure 2 shows the two main subsystems of g-LIMIT: the inertially isolated platform assembly and the base

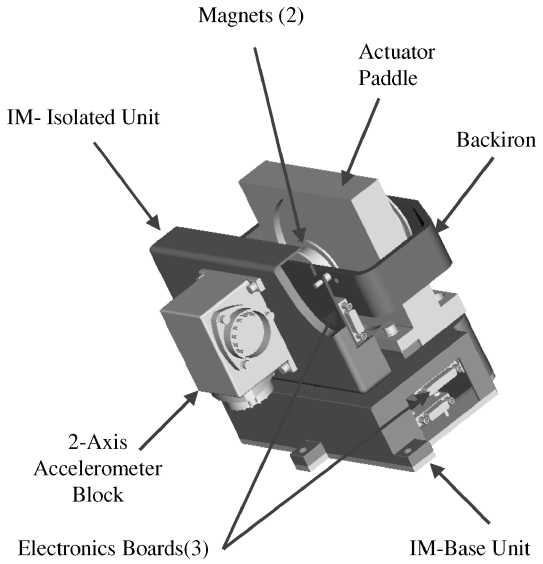

Fig. 3 Isolator module of g-LIMIT.

assembly that is rigidly attached to the MSG work volume floor. The base assembly footprint is approximately 0.396×0.345 m, whereas the diameter of the platform assembly is 0.345 m. At the nominal (or centered) position, the total height of g-LIMIT is 0.229 m. A dummy mass of 7.43 kg is mounted to the 10.5-kg isolated platform assembly for characterization testing. Three lockdown fasteners secure the isolator assembly to the base plate during transport, stowage, installation, and idle times.

A novel aspect of g-LIMIT is the modularity attained through the use of three isolator modules (IM), shown in Fig. 3. Each IM integrates together a dual-axis actuator, two axes of acceleration sensing, two axes of position sensing, and control electronics into one modular unit. Control forces are applied to the isolated assembly using non-contact Lorentz force actuators. The actuator comprises two subsystems; the backiron/permanent magnet assembly that forms a closed-flux-return path is mounted to the isolated platform assembly and a "paddle" that is mounted to the base assembly with two orthogonal sets of actuation coil windings. A commanded current in the paddle interacts with the magnetic field passing between the two magnets across the air gap to generate a force on the isolated platform assembly. Each actuator has two channels, one normal to the plane of the experiment mounting platform and one in the plane. With a scale factor of 0.8 N/m and a maximum current of 1.7 A per axis, the maximum force of 4.08 N is obtained by summing the three channels in the direction normal to the platform plane.

Another novel feature of g-LIMIT is the sensor that measures the relative motion of the isolated assembly with respect to the MSG-mounted base assembly. The patent-pending implicit position sensor uses a drive coil wound around the permanent magnets to induce a signal on the actuation coil for sensing relative motion much like a standard resolver. Inertial force-balanced proof mass accelerometers (AlliedSignal QA3000) are mounted to the electronics box on the backiron assembly to measure the inertial motion of the isolated platform. Together the relative position and acceleration measurements are used by the feedback control system to compute the current commands for the actuator. Three additional accelerometers are mounted to the base assembly for reference measurements.

To ensure that the magnet does not contact the paddle assemblies, a snubber system is integrated into the base plate and payload mounting structure (PMS). The snubber system uses pins attached to the circumference of the PMS and bumper blocks mounted on the base plate to provide mechanical rattle-space constraints. The bumper blocks and pins are designed to limit the relative displacement between the isolator assembly and the base assembly to ± 10 mm along the axis of the pins and in the direction normal to plane containing the three pins. Hence, the height varies from 0.218 to 0.239 m through the full range of vertical motion.

A set of utility umbilicals connects the isolated platform assembly to the base assembly to pass power and data between the MSG and the experiment. There are three umbilicals located at 120-deg intervals around the inner periphery of the isolated platform assembly at one end and the base assembly at the other end. A 90-degree bend between the base end and the isolated platform end is chosen rather than a full loop to minimize the umbilical stiffness.[1] Ground-test data were used to estimate the stiffness of each g-LIMIT flight umbilical as 4.7 and 6.5 N/m in the two translational axes in the plane of the umbilical.

B. Control System Architecture

The g-LIMIT system accomplishes inertial isolation using an acceleration feedback control system to sense the motion of the experiment and apply forces to reject the unwanted motion. An outer-loop (low-frequency) position feedback controller is used to center the platform in the sway space while commanding the platform to follow the quasi-steady motion of the vehicle. When relative position and absolute acceleration of the platform are sensed the active control system forces the platform to follow the very-low-frequency motion of the base and attenuating the base motion at higher frequencies.

The inner loop/outer loop architecture for the g-LIMIT control system is chosen so that the position loop will issue acceleration commands to be tracked by the high-gain acceleration loop. Because the accelerations are not always commanded to zero, the position loop actually disturbs the acceleration environment by forcing the platform to remain centered. However, the inner and outer loops are separated in the frequency domain such that the position control system only operates at very low frequencies. This architecture is used to reject accelerometer noise, accelerometer bias, and umbilical force bias, all of which are not directly measurable but manifest a position error. Through integral action, the position control system operates in the outer loop to reject these force and acceleration biases. At higher frequencies (above 0.01 Hz), the acceleration control system rejects the measured acceleration disturbances. Because of the potential interaction between the position and acceleration control loops, the position loop must be considered in the analysis and design of the acceleration control loop. The baseline control approach for g-LIMIT uses proportional-integral-derivative (PID) controllers for both loops.[3]

Whereas the position control operates in the outer loop to estimate and reject inner-loop biases and noise, the system has no means to distinguish position sensor noise and bias from environmental disturbances. Position sensor bias affects the home position about which the system is controlled and can potentially reduce the travel range in the direction of the bias. Sensor noise is a more significant issue than bias because the system will respond to position sensor noise and potentially violate the travel constraints. The dynamic response of the system to position sensor noise is addressed through designing the sensor for low noise and tuning the position control system. Position sensor noise tends not to be a significant impact in this case because of the low gain needed in the position control system.

Another controller architecture permitted by g-LIMIT software is a fully centralized multiple-input/multiple-output (MIMO) controller that has as its input both acceleration and position measurements. The position sensor measurements are sampled at 25 Hz, whereas the accelerations are sampled at 500 Hz, but this two-sample rate scenario can be adequately accommodated in a MIMO context by including the antialiasing filters on the relative position measurements. This is one means of frequency weighting that may be used to prevent interaction between the position and acceleration control in a fully centralized design.

However, the large dynamic range and large number of frequency weighting states required of a fully centralized MIMO design unnecessarily complicates the control design and could potentially lead to numerical issues. Whereas modern control tools are well suited to frequency-dependent designs of this nature, fully centralized control is unnecessary and undesirable in this context. In view of the simplicity and adequacy of a PID-type position controller in the

outer loop, this paper explores an architecture where a MIMO acceleration controller is designed for the inner loop and the baseline nominal PID position controller is implemented in the outer loop.

III. Control Design Approaches

Classical control methods are known to provide inherent robustness and simplicity of design and implementation. However, classical control methods are not well suited for multivariable (coupled) systems with parametric uncertainties. Such is the case with microgravity vibration isolation systems. Isolation systems cannot be tested in six degrees of freedom on the ground due to gravitational coupling; hence, the dynamic properties of the system are often poorly known before on-orbit operation. In some cases, only a lower limit is known for the structural frequencies of an experiment payload to be mounted to the isolation system. The combination of unknown payload characteristics and uncertain flexible umbilicals in the primary load path results in an uncertain multivariable dynamic system with stringent performance requirements.

A. Design for Nominal Performance

H_2 methods are often used when designing control systems to reduce the vibration response of a flexible structure. Whereas H_2 design gives good nominal performance, the controllers are highly tuned to the design model and errors in the design model are not accounted for, typically inducing instability in the presence of slight parameter variations with high authority controllers. Controller order reduction is also not routinely possible because of the sensitivity of the control gains. As a result, the actual performance achievable is limited with H_2 designs. To achieve high levels of performance in the presence of uncertainties associated with umbilical and payload (isolated experiment) dynamics, robustness to model errors must be taken into account in the design process.

Another approach to design for nominal performance employs the H_∞ norm, which can be interpreted as the gain of the system and is the worst-case amplification over all inputs $w(t)$ of unit energy. From a frequency-domain perspective, the H_∞ norm is defined as the maximum singular value of $\boldsymbol{T}(s)$ over all frequencies, that is,

$$\|\boldsymbol{T}_{zw}\|_\infty = \sup_\omega \{\bar{\sigma}[\boldsymbol{T}_{zw}(j\omega)]\} \tag{1}$$

Here $\boldsymbol{z}(t)$ is the vector of performance variables. H_∞ control design theory, based on Refs. 9 and 10, involves defining (possibly frequency-dependent) weights on the inputs and outputs such that the performance objectives are satisfied by minimizing $\|\boldsymbol{T}_{zw}\|_\infty$. Because the H_∞ norm is defined with respect to the peak magnitude of the transfer matrix frequency response and the H_2 norm is defined by an integral square quantity (in time or frequency by Parseval's theorem), the respective closed-loop systems typically have considerably different characteristics. With regard to mean-square performance requirements of microgravity vibration isolation, H_2 design is typically better suited for nominal performance than are H_∞ designs. The significant benefit of H_∞ theory, however, is that robustness to model errors is explicitly factored into the design process.

B. Design for Robust Stability

In addition to nominal performance, robust stability is an important design consideration. Robust stability requires the closed-loop system to remain stable in the presence of bounded model errors. The uncertainty may be modeled in many forms, such as multiplicative, inverse multiplicative, additive, parametric, etc., and may be located at various points in the loop. Because previous research has shown that the g-LIMIT control system stability is most sensitive to variations in the umbilical stiffness, a parametric uncertainty model is used herein to account for variations in the stiffness and damping of one umbilical. Additional details on the uncertainty model may be found in Ref. 11.

When all of the scalings and weights are absorbed into the plant P, the robust stability problem may be formulated as the linear fractional transformation (LFT) shown in Fig. 4a. The robust stability condition is based on the small gain theorem and states that if the uncertainties are scaled such that Δ_δ is the set of all proper and real

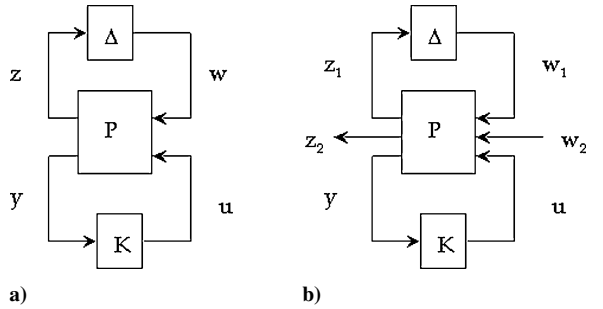

Fig. 4 LFT: a) robust stability and b) nominal performance/robust stability.

rational stable transfer matrices with $\|\Delta\|_\infty < \delta$ and assuming that $K(s)$ internally stabilizes the closed loop for $\Delta = 0$, then a sufficient condition for robust stability for all plants in the set formed by $\Delta \in \Delta_\delta$ is that[12]

$$\|\boldsymbol{T}_{zw}(K)\|_\infty \leq 1/\delta \tag{2}$$

Thus, like the nominal performance problem, robust stability is provided by minimizing the norm of a particular transfer function.

C. Design for Nominal Performance and Robust Stability

Whereas H_∞ (and μ-synthesis) methods provide both robust stability and robust performance in the presence of model errors, the performance is defined by an ∞-norm measure. A better approach from a mean-square performance perspective is mixed H_2/H_∞ optimization. The mixed H_2/H_∞ design procedure has been developed to provide robust stability and nominal (H_2) performance by minimizing the H_2 norm for one set of inputs/outputs while satisfying an ∞-norm overbound for another set of inputs/outputs. This mixed norm approach separates the optimization problem into two subproblems where the most appropriate norm is applied. For the inputs and outputs associated with performance, the H_2 norm is optimized while an upper limit on the ∞-norm is guaranteed for the inputs and outputs associated with the uncertainty model. With respect to Fig. 4b, the objective is to satisfy

$$\min_K \|T_{z2w2}\|_2 \tag{3}$$

subject to

$$\|T_{z1w1}\|_\infty < \gamma \tag{4}$$

The foundational work in mixed H_2/H_∞ design was done by Bernstein and Haddad,[13] who considered the case of one input and two outputs, with both full- and fixed-order control. The first attempt at solving the general mixed H_2/H_∞ problem was by Rotea and Khargonekar,[14] who allowed independent inputs and outputs for the two transfer functions and minimized the actual H_2 norm based on full state feedback. Ridgely et al. extended the formulation to output feedback including the fixed-order case with either regular or singular H_∞ constraints and provided a numerical solution in Refs. 15 and 16. Another approach to the general mixed H_2/H_∞ problem was developed by Sweriduk and Calise in Ref. 17, who used a differential games formulation to obtain fixed-order controllers. In Ref. 18, a homotopy algorithm was presented for the numerical solution of the necessary conditions of this formulation. The next section provides the mathematical framework for mixed H_2/H_∞ control design based on the method in Refs. 17 and 18. When D scales from μ-synthesis design are included, this approach is then applied to design mixed H_2/μ controllers for the g-LIMIT microgravity vibration isolation system.

IV. Mixed H_2/H_∞ Problem Formulation

The generalized plant of a standard control problem is given by

$$\dot{\boldsymbol{x}} = A\boldsymbol{x} + B_p\boldsymbol{w}_p + B_1\boldsymbol{w} + B_2\boldsymbol{u} \tag{5}$$

$$\boldsymbol{z}_p = C_p\boldsymbol{x} + D_{1p}\boldsymbol{u} \tag{6}$$

$$z = C_1 \boldsymbol{x} + D_{12} \boldsymbol{u} \tag{7}$$

$$\boldsymbol{y} = C_2 \boldsymbol{x} + D_{2p} \boldsymbol{w}_p + D_{21} \boldsymbol{w} + D_{22} \boldsymbol{u} \tag{8}$$

where $\boldsymbol{x} \in R^n$ is the state vector, $\boldsymbol{w}_p \in R^{nwp}$ and $\boldsymbol{z}_p \in R^{nzp}$ are the inputs and outputs defining the H_2 subproblem, $\boldsymbol{w} \in R^{nw}$ and $\boldsymbol{z} \in R^{nz}$ are the inputs and outputs defining the H_∞ subproblem, $\boldsymbol{u} \in R^{nu}$ is the control vector, and $\boldsymbol{y} \in R^{ny}$ is the measurement vector. Stabilizability, detectability, and standard rank conditions on the generalized plant are assumed.

To avoid the problem of overparameterization, a canonical form description for the controller can be used. It was shown in Ref. 19 that, if either a controller or observer canonical form is imposed on the compensator structure, the number of parameters is reduced to its minimal number. The internal structure of the compensator is prespecified by assigning a set of feedback invariant indices ν_i. In controller canonical form, the compensator is defined as

$$\dot{\boldsymbol{x}}_c = P^0 \boldsymbol{x}_c + N^0 \boldsymbol{u}_c - N^0 \boldsymbol{y} \tag{9}$$

$$\boldsymbol{u}_c = -P \boldsymbol{x}_c \tag{10}$$

$$\boldsymbol{u} = -H \boldsymbol{x}_c \tag{11}$$

where $\boldsymbol{x}_c \in R^{nc}$ and $\boldsymbol{u}_c \in R^{ny}$. P and H are free-parameter matrices, and P^0 and N^0 are fixed matrices of zeros and ones determined by the choice of controllability indices ν_i as follows:

$$P^0 = \text{block diag}\left\{ P_1^0, \ldots, P_{ny}^0 \right\} \tag{12}$$

$$P_i^0 = \begin{bmatrix} 0 & 1 & \cdots & 0 \\ \vdots & \ddots & \ddots & \vdots \\ \vdots & & \ddots & 1 \\ 0 & \cdots\cdots & & 0 \end{bmatrix}_{\nu_i \times \nu_i} \tag{13}$$

$$N^0 = \text{block diag}\left\{ [0 \cdots 01]^T_{1 \times \nu_i} \right\} \tag{14}$$

where $i = 1, \ldots, ny$. The controllability indices must satisfy the following condition:

$$\sum_i \nu_i = nc, \qquad i = 1, \ldots, ny \tag{15}$$

which imposes the lower bound $nc \geq ny$ on the order of the compensator.

When the canonical realization of the compensator dynamics is employed, augmenting the compensator states with the plant states allows the system to be formulated as a static gain optimization problem. Let

$$\bar{\boldsymbol{x}} = \begin{bmatrix} \boldsymbol{x} \\ \boldsymbol{x}_c \end{bmatrix} \tag{16}$$

$$\bar{\boldsymbol{u}} = \begin{bmatrix} \boldsymbol{u} \\ \boldsymbol{u}_c \end{bmatrix} \tag{17}$$

The augmented system may be expressed as

$$\dot{\bar{\boldsymbol{x}}} = \begin{bmatrix} A & 0 \\ -N^0 C_2 & P^0 \end{bmatrix} \bar{\boldsymbol{x}} + \begin{bmatrix} B_p \\ -N^0 D_{2p} \end{bmatrix} \boldsymbol{w}_p + \begin{bmatrix} B_1 \\ -N^0 D_{21} \end{bmatrix} \boldsymbol{w} + \begin{bmatrix} B_2 & 0 \\ -N^0 D_{22} & N^0 \end{bmatrix} \bar{\boldsymbol{u}} = \bar{A} \bar{\boldsymbol{x}} + \bar{B}_p \boldsymbol{w}_p + \bar{B}_1 \boldsymbol{w} + \bar{B}_2 \bar{\boldsymbol{u}} \tag{18}$$

$$\boldsymbol{z}_p = [C_p \quad 0] \bar{\boldsymbol{x}} + [D_{1p} \quad 0] \bar{\boldsymbol{u}} = \bar{C}_p \bar{\boldsymbol{x}} + \bar{D}_{1p} \bar{\boldsymbol{u}} \tag{19}$$

$$\boldsymbol{z} = [C_1 \quad 0] \bar{\boldsymbol{x}} + [D_{12} \quad 0] \bar{\boldsymbol{u}} = \bar{C}_1 \bar{\boldsymbol{x}} + \bar{D}_{12} \bar{\boldsymbol{u}} \tag{20}$$

$$\bar{\boldsymbol{y}} = [0 \quad I] \bar{\boldsymbol{x}} = \bar{C}_2 \bar{\boldsymbol{x}} \tag{21}$$

$$\bar{\boldsymbol{u}} = -\begin{bmatrix} H \\ P \end{bmatrix} \bar{\boldsymbol{y}} = -G \bar{\boldsymbol{y}} \tag{22}$$

Equations (18–22) define a static gain output feedback problem where the compensator is represented by a minimal number of free parameters in the design matrix G.

Consequently, the closed-loop system is given by

$$\dot{\bar{\boldsymbol{x}}} = (\bar{A} - \bar{B}_2 G \bar{C}_2) \bar{\boldsymbol{x}} + \bar{B}_p \boldsymbol{w}_p + \bar{B}_1 \boldsymbol{w} = \tilde{A} \bar{\boldsymbol{x}} + \tilde{B}_p \boldsymbol{w}_p + \tilde{B} \boldsymbol{w} \tag{23}$$

$$\boldsymbol{z}_p = (\bar{C}_p - \bar{D}_{1p} G \bar{C}_2) \bar{\boldsymbol{x}} = \tilde{C}_p \bar{\boldsymbol{x}} \tag{24}$$

$$\boldsymbol{z} = (\bar{C}_1 - \bar{D}_{12} G \bar{C}_2) \bar{\boldsymbol{x}} = \tilde{C} \bar{\boldsymbol{x}} \tag{25}$$

For the H_2 subproblem, the objective is to minimize the H_2 norm of the closed-loop transfer function from disturbance inputs $\boldsymbol{w}_p$ to performance outputs $\boldsymbol{z}_p$:

$$T_{zpwp} = \tilde{C}_p (sI - \tilde{A})^{-1} \tilde{B}_p \tag{26}$$

where the disturbances are confined to the set of signals with bounded power and fixed spectra. For the H_∞ subproblem, the objective is to minimize the H_∞ norm of the transfer function from disturbance inputs $\boldsymbol{w}$ to performance outputs $\boldsymbol{z}$. The performance index for the mixed H_2/H_∞ problem is a weighted combination of the Lagrangian for the H_2 problem and the Lagrangian for the H_∞ problem and is given by[17]

$$\mathcal{L} = \text{tr}\left\{ Q_\infty \tilde{B} \tilde{B}^T + \left(\tilde{A}^T Q_\infty + Q_\infty \tilde{A} + \tilde{C}^T \tilde{C} + \gamma^{-2} Q_\infty \tilde{B} \tilde{B}^T Q_\infty \right) L + \lambda X \tilde{C}_p^T \tilde{C}_p + \left(\tilde{A} X + X \tilde{A}^T + \tilde{B}_p \tilde{B}_p^T \right) L_p \right\} \tag{27}$$

The weight λ on the H_2 norm allows a tradeoff between (H_2) performance and the H_∞ norm. Matrix gradients are taken to obtain the first-order necessary conditions:

$$\frac{\partial \mathcal{L}}{\partial Q_\infty} = \left(\tilde{A} + \gamma^{-2} \tilde{B} \tilde{B}^T Q_\infty \right) L + L \left(\tilde{A} + \gamma^{-2} \tilde{B} \tilde{B}^T Q_\infty \right)^T + \tilde{B} \tilde{B}^T = 0 \tag{28}$$

$$\frac{\partial \mathcal{L}}{\partial L} = \tilde{A}^T Q_\infty + Q_\infty \tilde{A} + \tilde{C}^T \tilde{C} + \gamma^{-2} Q_\infty \tilde{B} \tilde{B}^T Q_\infty = 0 \tag{29}$$

$$\frac{\partial \mathcal{L}}{\partial X} = \tilde{A}^T L_p + L_p \tilde{A} + \lambda \tilde{C}_p^T \tilde{C}_p = 0 \tag{30}$$

$$\frac{\partial \mathcal{L}}{\partial L_p} = \tilde{A} X + X \tilde{A}^T + \tilde{B}_p \tilde{B}_p^T = 0 \tag{31}$$

$$\frac{\partial \mathcal{L}}{\partial G} = 2 \left[\bar{D}_{12}^T \bar{D}_{12} G \bar{C}_2 L \bar{C}_2^T - \bar{D}_{12}^T \bar{C}_1 L \bar{C}_2^T - \bar{B}_2^T Q_\infty L \bar{C}_2^T - \lambda \bar{D}_{1p}^T \bar{C}_p X \bar{C}_2^T + \lambda \bar{D}_{1p}^T \bar{D}_{1p} G \bar{C}_2 X \bar{C}_2^T - \bar{B}_2^T L_p X \bar{C}_2^T \right] = 0 \tag{32}$$

A homotopy algorithm is presented in Ref. 18, which solves these necessary conditions and computes a family of mixed H_2/H_∞ compensators for varying weights γ and λ. The homotopy algorithm for fixed-order mixed H_2/H_∞ design also generates H_2, μ, and H_2/μ controllers of fixed dimension as special cases. This homotopy algorithm is a two-parameter iterative scheme that effectively trades between robust stability and nominal performance by varying the overbound on the ∞ norm and the weight on the H_2 cost in the mixed-norm cost functional. For a fixed γ overbound, the weight on the H_2 cost, λ, is increased until either the ∞-norm constraint becomes an active, equality constraint or until the H_2 norm ceases to decrease. Solutions where the ∞-norm constraint is active (at which point the H_2 norm can no longer be reduced) are called boundary solutions, the set of which provides an explicit Pareto optimal trade between nominal performance and robust stability. When the D scales from μ-synthesis are incorporated into the H_∞ subproblem, the structure of the uncertainty block may be accounted for, resulting in the fixed-order mixed H_2/μ design procedure used in the following section.

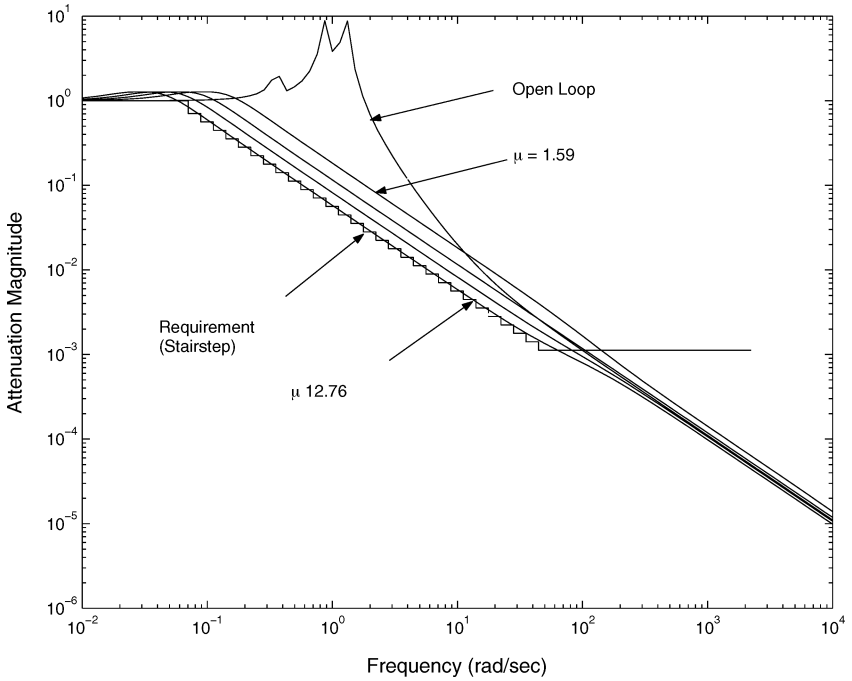

Fig. 5 Nominal attenuation performance with H_2 designs.

V. Control Design Results

Several aspects of the g-LIMIT microgravity vibration control application make the fixed-order mixed H_2/μ design procedure particularly apropos. The primary control objective for g-LIMIT is to satisfy the officially documented flight project performance requirement,[8] which is shown against the design results in Fig. 5. Robustness is an obvious design issue as well, one that must be addressed while meeting the performance requirement. The mixed H_2/μ design method provides just that: It maximizes stability robustness to bounded model errors for a given level of mean-square performance. Likewise, nominal performance can be maximized while guaranteeing a specified level of robust stability.

Controller state dimension is also a significant implementation issue for g-LIMIT. Standard H_2 and H_∞ design approaches yield full-order compensators with the dimension of the generalized plant, including weighting function states and D scale states for μ synthesis. Generalized plant dimension is especially significant in this case because of the controller architecture. Including the closed-position loop in the generalized plant as shown in Fig. 3 increases the dimension of the generalized plant and, hence, the dimension of the full-order H_2 and H_∞ controllers.

This is a good example of superfluous controller states arising from the methodology rather than the design process. With six PID position controllers in the outer loop, the full-order MIMO acceleration controller will have 12 states due strictly to the architecture. The nominal plant dynamics has a minimum of 18 states (6 position, 6 velocity, and 6 for acceleration output filters). Because the flight computer throughput limits the controller to 35 states, the remaining 5 states available for design weights is clearly insufficient if full-order design is to be used. Stability and performance properties are not generally retained if the controller order must be reduced to a degree that can be implemented. That is especially true in this case because of the stringent performance requirements of microgravity vibration isolation. The fixed-order mixed-norm method addresses this limitation of standard robust control by synthesizing MIMO acceleration controllers with a specified dimension that is an integer multiple of the number of measurements; for example, 6, 12, 18, etc., states.

By enforcing the order constraints in the fixed-order mixed H_2/μ design procedure, robust stability can be maximized for a given level of mean-square performance with controllers that can be implemented in flight hardware. More than simply demonstrating the utility of this methodology, the microgravity vibration isolation application justifies the significance of this approach.

A. H_2 Designs

The generalized plant for control design is shown in Fig. 6. For H_2 design, the disturbance inputs include the three translational base accelerations $\boldsymbol{w}_{\text{acc}}$, three directly applied forces $\boldsymbol{w}_{\text{fd}}$, and six elements of the accelerometer noise vector $\boldsymbol{n}_{\text{acc}}$. The performance outputs include weighted platform acceleration $\boldsymbol{z}_{\text{acc}}$, weighted position control signal $\boldsymbol{z}_{pu}$, and weighted acceleration control $\boldsymbol{z}_u$. As a consequence of the control architecture described in the last section, the input to the control system is the acceleration error, which is the difference in platform acceleration measurement and the acceleration command generated by the baseline PID position controller. Six actuator forces comprise the control input vector. The g-LIMIT flight hardware includes analog antialiasing filters, which are represented in this design as a second-order filter with a 125-Hz break frequency on the acceleration measurement and a single 10-Hz low-pass filter on position measurements.

To assess nominal performance, a metric denoted attenuation factor is defined for each controller as the maximum value of the ratio of achieved performance to the required performance over the frequency range of interest:

$$\text{attenuation factor} = \sup_{\omega_{\text{low}} < \omega < \omega_{\text{high}}} \left\{ \frac{\bar{\sigma}\left[T_{\ddot{x}_p \ddot{x}_b}(j\omega)\right]_{\text{cl}}}{\bar{\sigma}\left[T_{\ddot{x}_p \ddot{x}_b}(j\omega)\right]_{\text{req}}} \right\} \tag{33}$$

where the p subscript indicates platform acceleration and the b subscript indicates the base (ISS) disturbance acceleration. Performance here is defined as the maximum singular value of the closed-loop transfer function from ISS translational accelerations to the isolated platform translational acceleration. The frequency range of interest is not exactly arbitrary, but is chosen as the range from 0.01 to 3 Hz. (Slight exceedances are allowed below 0.01 Hz and around 10 Hz, the latter due to limiting the controller state dimension.) This range provides a consistent comparison across controllers designed with different methods. (Note that the results are slightly exaggerated for low-authority controllers due to the resonant amplification at the break frequency.) Using this performance metric provides a scalar measure of nominal performance akin to the scalar μ measure for robust stability analysis. Controllers with attenuation

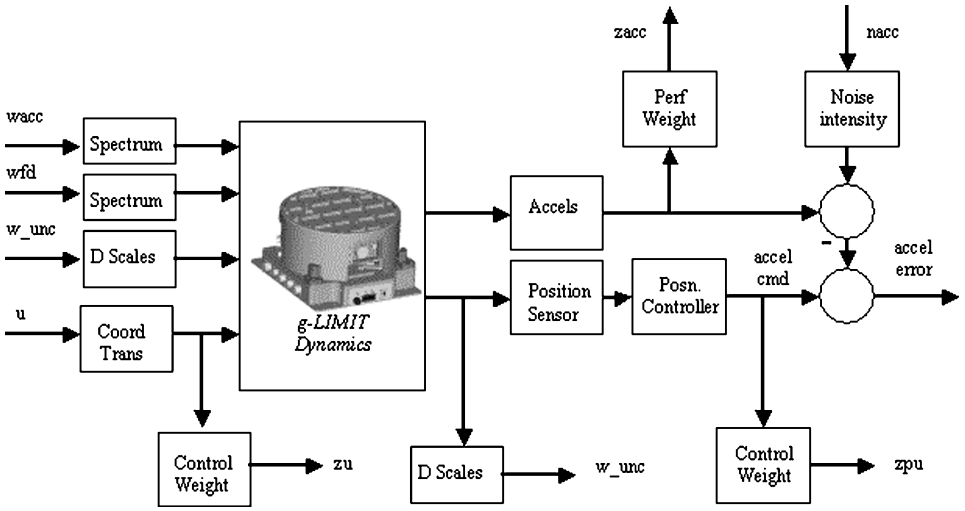

Fig. 6 Generalized plant for control design of g-LIMIT.

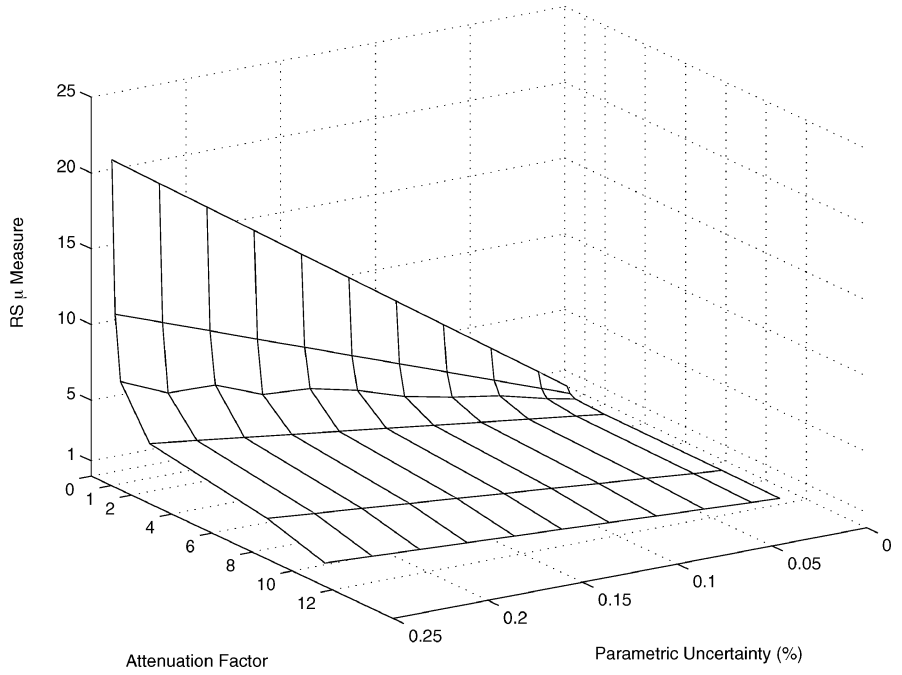

Fig. 7 Robust stability of H_2 designs as a function of parametric uncertainty.

factors greater than one fail to meet the performance requirement, whereas controllers with attenuation factors less than one exceed the requirement.

A set of H_2 control designs is designed for varying levels of performance and control authority by varying W_p in the acceleration performance weight:

$$W_{p,\,\text{accel}} = (W_p)/(0.0032s + 1) \tag{34}$$

which penalizes accelerations up to 50 Hz. Figure 5 presents the nominal performance of the full-order, 54-state H_2 control designs at varying levels of attenuation performance. For each curve, the corresponding peak μ measure is shown where robust stability is assessed with respect to 10% real parametric uncertainty in the umbilical stiffness. Nominal performance is defined by the attenuation of base accelerations on the isolated platform and is compared against the performance requirement shown in Fig. 5. Controller order reduction for these 54 state H_2 controllers was not possible: Even slight reductions in controller order resulted in unstable controllers for each level of nominal performance.

Robust stability substantially degrades as the attenuation performance improves with these designs. Figure 5 indicates that the nominal performance requirement is met with a design that has a μ measure of 12.76 (for 10% uncertainty), which indicates that a destabilizing perturbation in umbilical stiffness exists with a magnitude of less than 1%. Figure 7 presents a surface of peak μ values for each H_2 controller evaluated for real parameter variation in umbilical stiffness and damping varied up to 25%. Clearly demonstrated in Figs. 5 and 7 is the significant loss of robust stability as a function of uncertainty for a given H_2 controller and in general as a function of attenuation performance for the H_2 methodology. In general, only the lowest performing controllers (attenuation factors greater than 4) satisfy the robust stability test for the very low levels of parameter variation (5% or less).

B. Fixed-Order Mixed H_2/μ Designs

Next, a set of 12th-order mixed H_2/μ controllers are synthesized for comparison to the 54-state full-order H_2 controllers. For this design, the H_2 optimization problem from the last section is augmented

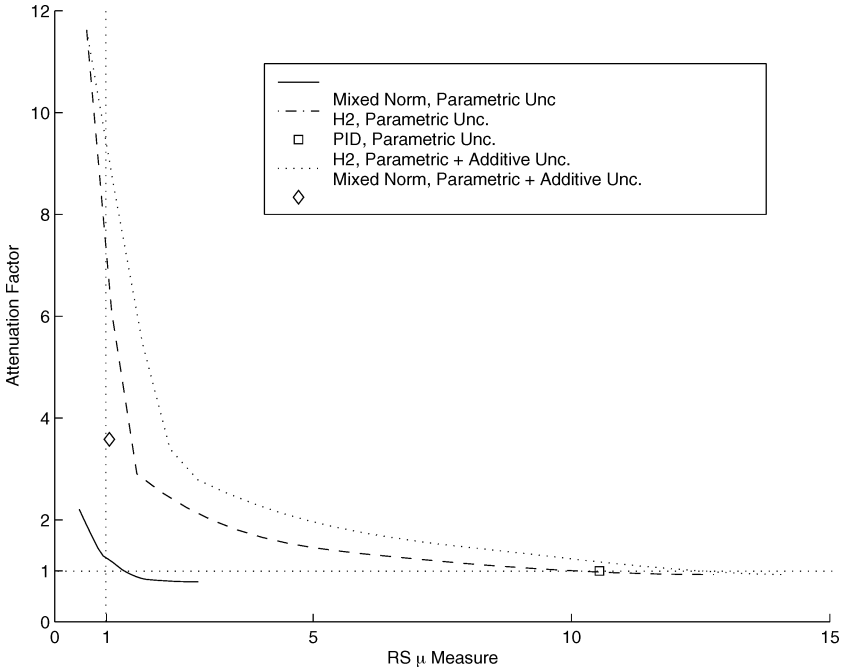

Fig. 8 Performance and robustness trade.

with an H_∞ subproblem based on the umbilical stiffness and damping parametric uncertainty model.[6] The two subproblems of the mixed-norm design are defined by the inputs and outputs:

$$\boldsymbol{w}_2 = \begin{bmatrix} \boldsymbol{n}_{\text{acc}} \\ \boldsymbol{w}_{\text{acc}} \\ \boldsymbol{w}_{\text{fd}} \end{bmatrix}, \qquad \boldsymbol{z}_2 = \begin{bmatrix} \boldsymbol{z}_{\text{acc}} \\ \boldsymbol{z}_u \\ \boldsymbol{z}_{pu} \end{bmatrix}$$

$$\boldsymbol{w}_\infty = [\boldsymbol{w}_{\text{unc}}], \qquad \boldsymbol{z}_\infty = [\boldsymbol{z}_{\text{unc}}]$$

where the uncertain inputs and outputs $\boldsymbol{w}_{\text{unc}}$ and $\boldsymbol{z}_{\text{unc}}$ are associated with the uncertain umbilical stiffness and damping. The mixed-norm controllers are obtained by varying the H_2 performance weight in the same manner as the full-order H_2 designs. The same weights were used for the H_2 subproblem as for the full-order H_2 designs with the exception of the performance weight range. When the 54 state H_2 controller is compared to the 12th-order mixed H_2/μ design for the same H_2 weights, the attenuation factor degrades from 0.95 for the H_2 design to 1.51 for the mixed H_2/μ design, whereas the peak μ measure improves from 12.76 to 0.90. Whereas the performance only slightly decreases with the addition of robust stability and controller order constraints in the optimization process, the robust stability increases substantially. Hence, slightly higher performance weights were needed to achieve the same level of nominal attenuation performance with the mixed-norm designs. This loss of performance for a given set of weights is a direct result of the added constraints of the H_∞ cost and possibly the fixed controller order.

Attenuation performance for the full set of performance weights with the mixed-norm design is similar to the nominal performance for the strict H_2 controllers shown in Fig. 5. However, the peak μ values are much lower through the full range of performance with the mixed H_2/μ controllers than with the full-order H_2 controllers for a given level of attenuation performance. This significant benefit of the mixed H_2/μ method in comparison to H_2 design is revealed in Fig. 8. The improvement in robust stability (assessed for 10% real parametric uncertainty) for the same levels of performance is indicated by the performance and stability trade curves for both the H_2 controllers and mixed H_2/μ methodologies. A substantially better trade space is obtained for the 12th-order mixed H_2/μ controllers than for the 54th-order H_2 designs. The same levels of performance are obtained with considerably greater robust stability with the mixed-norm designs. For completeness, the performance and robust stability of the baseline PID controller is indicated as well. Interestingly, the PID controller lies on the design curve for the H_2 designs, which indicates that the same levels of performance and stability can be attained with the PID controller as with the H_2 designs.

In addition to the real parameter uncertainty, a mixed H_2/μ controller was designed for additive uncertainty as well. In this case, an additive uncertainty model given by

$$W_{\text{add}} = 0.001\frac{(1.2566s + 1)}{(0.0251s + 1)} \tag{35}$$

was included to provide robustness to unmodeled modes above 35 Hz (representing potential payload dynamics). The performance and stability of this controller is indicated in Fig. 8 along with the set of H_2 controllers evaluated for this parametric and additive uncertainty model.

This type of analysis is important to determine the range of acceptable controllers in terms of nominal performance and robust stability. Figure 8 shows the region of acceptable controllers for a specified level of uncertainty (10% in this case). The vertical dashed line is the boundary of acceptable controllers in terms of stability robustness, whereas the horizontal dashed line delineates the acceptable performance region. Controllers above the horizontal line fail the stability requirement, whereas controllers to the right of the vertical line fail the attenuation performance criteria. Note, however, that even though the mixed H_2/μ designs are far superior to the H_2 designs, the nominal performance objective is not satisfied for any controller with a μ measure less than one. The performance requirement cannot be satisfied with guaranteed stability for 10% real parameter uncertainty with this design set.

VI. Conclusions

Previous approaches to microgravity vibration isolation system designs have utilized strictly classical methods with the exception of a few studies using H_2 and H_∞ methods. In this paper, H_2 and mixed H_2/μ methods have been shown to result in comparable levels of nominal performance, albeit at significantly different levels of robustness. An uncertainty model for microgravity vibration isolation controller design with respect to parametric uncertainties in umbilical stiffness was used for robust stability analysis and robust control design.

This paper presents a control design approach that is well suited to the stringent performance and stability requirements of microgravity vibration isolation. Standard full-order H_2 and H_∞ designs do not simultaneously provide good mean-square performance and robust stability guarantees with controllers of low enough order to be implemented in flight hardware. Note that, in this application, the low compensator order was necessary due to implementation constraints. Incorporating D scales results in a fixed-order mixed H_2/μ design approach for which controllers are synthesized and analyzed to determine the maximum robust stability attainable subject to a nominal performance requirement. Using the fixed-order mixed H_2/μ design approach resulted in controllers of low order that virtually recovered the nominal performance of the full-order H_2 controllers with the robust stability guarantees of the full-order μ controller.

References

[1]Edberg, D. L., and Wilson, B. W., "Design and Testing of Reduced-Stiffness Umbilicals for Space Station Microgravity Isolation," AIAA Paper 2000-1408, April 2000.

[2]Grodsinsky, C. M., and Whorton, M. S., "Survey of Active Vibration Isolation Systems for Microgravity Applications," *Journal of Spacecraft and Rockets*, Vol. 37, No. 5, 2000, pp. 586–596.

[3]Jackson, M., Kim, Y., and Whorton, M. S., "Design and Analysis of the g-LIMIT Baseline Vibration Isolation Control System," AIAA Paper 2002-5019, Aug. 2002.

[4]Hyde, T., and Crawley, E., "H_2 Synthesis for Active Vibration Isolation," *Proceedings of the 1995 American Control Conference*, IEEE Publications, Piscataway, NJ, 1995, pp. 3835–3839.

[5]Hampton, R. D., and Whorton, M. S., "Frequency-Weighting Filter Selection, for H2 Control of Microgravity Isolation Systems: A Consideration of the 'Implicit Frequency Weighting' Problem," *IEEE Transactions on Instrumentation and Measurement*, Vol. 49, No. 2, 2000, pp. 265–269.

[6]Whorton, M. S., "Robust Control for Microgravity Vibration Isolation With Parametric Uncertainty,"*Proceedings of the 2002 American Control Conference*, IEEE Publications, Piscataway, NJ, 2002, pp. 256–261.

[7]Fialho, I. J., "H-Infinity Control Design for the Active Rack Isolation System," *Proceedings of the 2000 American Control Conference*, IEEE Publications, Piscataway, NJ, 2000, pp. 2082–2086.

[8]Whorton, M. S., "g-LIMIT: A Microgravity Vibration Isolation System for the International Space Station," AIAA Paper 2001-5090, Oct. 2001.

[9]Frances, B. A., *A Course in H_∞ Control Theory*, Springer-Verlag, Berlin, 1987.

[10]Doyle, J. C., Glover, K., Khargonekar, P., and Francis, B. A., "State-Space Solutions to Standard H_2 and H_∞ Control Problems," *IEEE Transactions on Automatic Control*, Vol. 34, No. 8, 1989, pp. 831–847.

[11]Kim, Y. K., and Whorton, M. S., "Equations of Motion for the g-LIMIT Microgravity Vibration Isolation System," NASA TM-2001-211301, Oct. 2001.

[12]Zhou, K., Doyle, J.C., and Glover, K., *Robust and Optimal Control*, Prentice–Hall, Upper Saddle River, NJ, 1996, pp. 217–219.

[13]Bernstein, D. S., and Haddad, W. M., "LQG Control with an H_∞ Performance Bound: A Riccati Equation Approach," *IEEE Transactions on Automatic Control*, Vol. AC-34, 1989, pp. 293–305.

[14]Rotea, M., and Khargonekar, P. P., "H_2-Optimal Control with an H_∞ Constraint: The State Feedback Case," *Automatica*, Vol. 27, No. 2, 1991, pp. 307–316.

[15]Ridgely, D. B., Mracek, C. P., and Valavani, L., "Numerical Solutions to the General Mixed H_2/H_∞ Optimization Problem," *Proceedings of the 1992 American Control Conference*, IEEE Publications, Piscataway, NJ, 1992, pp. 1353–1357.

[16]Ridgely, D. B., Valavani, L., Dahleh, M., and Stein, G., "Solutions to the General Mixed H_2/H_∞ Control Problem—Necessary Conditions for Optimality," *Proceedings of the 1991 American Control Conference*, IEEE Publications, Piscataway, NJ, 1992, pp. 1348–1352.

[17]Sweriduk, G. D., and Calise, A. J., "A Differential Game Approach to the Mixed H_2/H_∞ Problem," *Proceedings of the 1994 AIAA Guidance, Navigation and Control Conference*, AIAA, Washington, DC, 1994, pp. 1072–1082.

[18]Whorton, M. S., Buschek, H., and Calise, A. J., "Homotopy Algorithm for Fixed-Order Mixed H_2/H_∞ Design," *Journal of Guidance, Control, and Dynamics*, Vol. 19, No. 6, 1996, pp. 1262–1269.

[19]Kramer, F. S., and Calise, A. J., "Fixed-Order Dynamic Compensation for Multivariable Linear Systems," *Journal of Guidance, Control, and Dynamics*, Vol. 11, No. 1, 1988, pp. 80–85.

M. Lake
Associate Editor